

Northumbria Research Link

Citation: Wang, Wei-Lin, Liu, Qiang, Liu, Zhao-Yang, Wu, Qiang and Fu, Yong Qing (2022) Simulation of a Temperature-Compensated Voltage Sensor Based on Photonic Crystal Fiber Infiltrated with Liquid Crystal and Ethanol. *Sensors*, 22 (17). p. 6374. ISSN 1424-8220

Published by: MDPI

URL: <https://doi.org/10.3390/s22176374> <<https://doi.org/10.3390/s22176374>>

This version was downloaded from Northumbria Research Link: <https://nrl.northumbria.ac.uk/id/eprint/49955/>

Northumbria University has developed Northumbria Research Link (NRL) to enable users to access the University's research output. Copyright © and moral rights for items on NRL are retained by the individual author(s) and/or other copyright owners. Single copies of full items can be reproduced, displayed or performed, and given to third parties in any format or medium for personal research or study, educational, or not-for-profit purposes without prior permission or charge, provided the authors, title and full bibliographic details are given, as well as a hyperlink and/or URL to the original metadata page. The content must not be changed in any way. Full items must not be sold commercially in any format or medium without formal permission of the copyright holder. The full policy is available online: <http://nrl.northumbria.ac.uk/policies.html>

This document may differ from the final, published version of the research and has been made available online in accordance with publisher policies. To read and/or cite from the published version of the research, please visit the publisher's website (a subscription may be required.)






**Northumbria
University**
NEWCASTLE



UniversityLibrary

Article

Simulation of a Temperature-Compensated Voltage Sensor Based on Photonic Crystal Fiber Infiltrated with Liquid Crystal and Ethanol

Wei-Lin Wang ¹, Qiang Liu ^{1,2,*}, Zhao-Yang Liu ³, Qiang Wu ⁴ and Yong-Qing Fu ⁴¹ School of Control Engineering, Northeastern University at Qinhuangdao, Qinhuangdao 066004, China² Hebei Key Laboratory of Micro-Nano Precision Optical Sensing and Measurement Technology, Qinhuangdao 066004, China³ College of Precision Instruments and Optoelectronic Engineering, Tianjin University, Tianjin 300072, China⁴ Faculty of Engineering and Environment, Northumbria University, Newcastle upon Tyne NE1 8ST, UK

* Correspondence: liuqiang@neuq.edu.cn

Abstract: A simulated design for a temperature-compensated voltage sensor based on photonic crystal fiber (PCF) infiltrated with liquid crystal and ethanol is presented in this paper. The holes distributed across the transverse section of the PCF provide two channels for mode coupling between the liquid crystal or ethanol and the fiber core. The couplings are both calculated accurately and explored theoretically using the finite element method (FEM). The influence of voltage on the alignment of the liquid crystal molecules and confinement loss of the fiber mode are studied. Liquid crystal molecules rotate which changes its properties as the voltage changes. As the characteristics of the liquid crystal will be affected by temperature, therefore, we further fill using ethanol, which is merely sensitive to temperature, into one hole of the PCF to realize temperature compensation. The simulated results show that the sensitivity is up to 1.29977 nm/V with the temperature of 25 °C when the voltage ranges from 365 to 565 V. The standard deviation of the wavelength difference is less than 2 nm within the temperature adjustment from 25 to 50 °C for temperature compensation. The impacts of the construction parameters of the PCF on sensing performances of this voltage sensor are also analyzed in this paper.

Keywords: photonic crystal fiber; voltage sensor; liquid crystal; mode coupling; finite element method; temperature compensation



Citation: Wang, W.-L.; Liu, Q.; Liu, Z.-Y.; Wu, Q.; Fu, Y.-Q. Simulation of a Temperature-Compensated Voltage Sensor Based on Photonic Crystal Fiber Infiltrated with Liquid Crystal and Ethanol. *Sensors* **2022**, *22*, 6374. <https://doi.org/10.3390/s22176374>

Academic Editors: Benjamin L. Miller and Francesco De Leonadis

Received: 5 July 2022

Accepted: 22 August 2022

Published: 24 August 2022

Publisher's Note: MDPI stays neutral with regard to jurisdictional claims in published maps and institutional affiliations.



Copyright: © 2022 by the authors. Licensee MDPI, Basel, Switzerland. This article is an open access article distributed under the terms and conditions of the Creative Commons Attribution (CC BY) license (<https://creativecommons.org/licenses/by/4.0/>).

1. Introduction

In this high-speed information age, more sensors with fast transmission, large capacity, high electromagnetic interference resistance, and compact size are needed. Due to these strengths, the optical fiber sensing technology has rapidly developed, bringing more opportunities for optical communication, optical sensing, and many other fields. In the last 20 years, a novel type of optic fiber named photonic crystal fiber (PCF) has been emerging rapidly which is generally made up of just one medium. The microstructure cladding of PCFs is lined with a periodic series of wavelength-scaled air holes that are densely packed in the two-dimensional direction while maintaining the same axial structure [1]. Compared with other conventional optical fibers, the diversity in the structure design of the PCFs is particularly abundant [2]. As the substrate materials are not environmentally sensitive, the different environmentally sensitive materials are filled into these air holes to create sensors with high sensitivity.

In 1954, J.R. Pierce first proposed the concept of mode coupling in the electromagnetic field during the discussion of the application of traveling wave tubes [3]. Later in the 1970s, A.W. Snyder [4], D. Marcuse [5], and A. Yariv [6] introduced the mode-coupling theory into the optical waveguide. Ever since, the mode-coupling theory has been widely used in the

optical waveguide to make optical devices, such as waveguide directional couplers [7–9], fiber optic couplers [10], distributed feedback lasers [11], and so on. The mode coupling effect in optical fibers produces a peculiar optical phenomenon and presents excellent optical properties. In recent years, special optical fibers based on the mode coupling effect show unique advantages in confinement loss, dispersion, and nonlinearity, and have been extensively adopted for a large collection of application areas in optical fiber communication and optoelectronic systems. Particularly, mode coupling theory gradually gains attention in fiber sensors. Filling sensitive materials into PCF brings diverse structures, in which another mode is exhibited and the coupling resonance with the fiber mode occurs when waveguide phase matches.

Liquid crystal (LC), as a material sensitive to temperature, electric field, and magnetic field, has been gradually applied in photonic crystal fiber sensors. In addition, LC has birefringent optical properties like crystal [12], which makes great contributions to the sensor sensitivity. Larsen and Bjarklev et al. from the Danish Institute of Technology were the first to fill liquid crystal into photonic crystal fibers to make fiber sensors. Through controlling the temperature and electric field, they proposed the concept of optical switch [13]. In 2009, Lei Wei developed an LC-filled PBG-PCF using negative permittivity, which could realize electronic and temperature control tuning. At the voltage value of 200 Vrms, the control temperature range was 20–80 °C and the bandgap change was 396 nm [14]. In 2015, Hu and Fu et al. put forward an all-fiber Mach–Zehnder interferometer on the basis of liquid crystal filling. They filled the core of a hollow PCF with LC and welded single-mode optical fibers on both ends of the filled PBG-PCF to make a Mach–Zehnder interferometer, reaching a temperature sensitivity of up to $-1.55 \text{ nm}/^\circ\text{C}$ [15]. It can be seen that the LC-filled PCFs could expand the application function of such fibers. In this paper, LC is infiltrated into one hole of the PCF to realize the voltage sensor by the coupling between the LC mode and fiber mode.

Voltage sensors are widely applied in power distribution systems, cables, electric machinery, and so on. In order to develop voltage sensors with high performances, research on the electro-optic effect [16–18], electro-strictive effect [19–21], and so on, are generally studied. Fiber voltage sensors have been widely put into application in various sensing sectors due to numerous distinctive qualities, including small weight, rapid reaction, and capability of remote operation. As the voltage surpasses the threshold, the LC molecules inside the air holes spin towards the presence of an electric field. Plenty of studies have been devoted to development of electric optical fiber devices filled with nematic liquid crystal (NLC). Haakestad et al. filled liquid crystal into a refractive-index-directed PCF to obtain a bandgap-guided fiber with a millisecond electrical reaction time [22]. Ertman et al. injected LC into a high-index PCF, enabling them to alter the phase birefringence adjustment at $0\sim 2 \times 10^{-4}$ [23]. Du et al. developed an electrically tunable filter in which the LC was loaded into PCF in a Sagnac loop with a tuning range of roughly 26 nm, reaching a sensitivity of 0.53 nm/V [24]. Huang et al. developed an electro-optical modulation established on the resonance principle, using LC injected into a PCF. The modulation range is between 1414 and around 1700 nm, reaching a sensitivity of 5.594 nm/V [25]. Our research group has undertaken some research on the electrical sensing characteristics based on PCF infiltrated with LC [26–28]. However, the temperature stability and reliability are not studied adequately, and the measurement range is not wide enough. Therefore, the voltage sensors based on PCF filled with LC are worth pursuing and in urgent need of development.

In this paper, the finite element method (FEM) based on the COMSOL Multiphysics software is applied to analyze the sensing performances of the PCF infiltrated with functional materials. The fiber mode and LC mode couple with each other as the phase matches. As we change the voltage of ambient environment, ranging from 365 to 565 V, the confinement loss and the resonance wavelength change simultaneously by which voltage can be detected. However, the characteristics of LC would be affected by temperature which would interference with sensor performance. Therefore, ethanol, which is merely sensitive

to temperature, is infiltrated into one hole of the PCF to realize temperature compensation. Meanwhile, the geometrical parameters of the PCF on the sensing characteristics are studied.

2. Structure of PCF and Material Parameters

The transverse section of proposed PCF infiltrated with LC and ethanol in this paper is clearly depicted in Figure 1. The red hole with nematic LC filled in has a diameter of $d_1 = 1.4 \mu\text{m}$. The two larger stomata in the x-direction have a diameter of $d_2 = 2.2 \mu\text{m}$ and other stomata are denoted by $d = 1.4 \mu\text{m}$ and have a refractive index of 1.0 by which the PCF is a polarization maintaining fiber and possesses high birefringence. The yellow hole in the symmetric position is filled with ethanol, which is utilized to compensate for temperature drift problems. The triangular-lattice distribution is chosen whose spacing is characterized by $\Lambda = 3 \mu\text{m}$. Radiation absorbers based on border conditions of the perfectly matched layer (PML) are utilized for completely assimilating the radiant vitality within the external area.

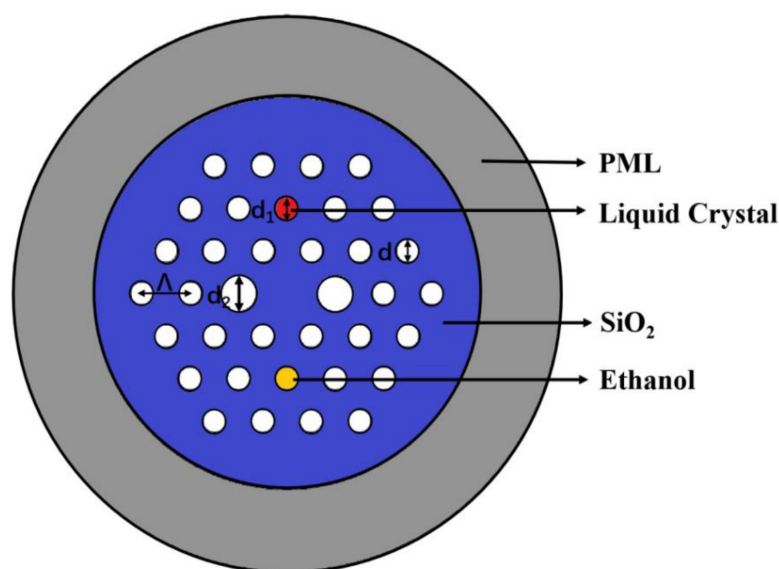


Figure 1. The transverse section of the proposed PCF infiltrated with liquid crystal and ethanol.

This structure of the PCF infiltrated with functional materials is designed to study its sensing characteristics. The preparation technology of the polarization maintaining PCF is very mature with the stacking method; therefore, it is not difficult to obtain the structure of this PCF. According to the existing filling methods, the capillary method is the most commonly used to fill LC into the air holes. In this paper, we selectively fill LC, which can be a little more difficult than full filling. We can use the laser perforation method [29]. A single-mode fiber is first fused to the PCF, then we use a laser to cut the single-mode fiber. Next, a femtosecond laser is used to punch holes in the cross-section of the single-mode fiber, so that the holes made are in series with the air holes to be filled. Thus, we can achieve selective filling based on the liquid full-filled method.

The backing material of the PCF is pure quartz (SiO_2), the dispersion of which is defined by the Sellmeier Equation as shown in Equation (1) [30]:

$$n^2 = 1 + \frac{0.6961663\lambda^2}{\lambda^2 - (0.0684043)^2} + \frac{0.4079426\lambda^2}{\lambda^2 - (0.1162414)^2} + \frac{0.8974794\lambda^2}{\lambda^2 - (9.896161)^2} \quad (1)$$

In this structure, the nematic LC E_7 , which is filled in the red hole, is an anisotropic liquid. LC E_7 forms a rod-like structure, which can be described in terms of ordinary refractive index n_o and extraordinary refractive index n_e . n_o and n_e are calculated using Equation (2) [31]:

$$n_{o,e} = A_{o,e} + \frac{B_{o,e}}{\lambda^2} + \frac{C_{o,e}}{\lambda^4} \quad (2)$$

where $A_o = 1.4994$, $B_o = 0.007$, $C_o = 0.0004$, $A_e = 1.6933$, $B_e = 0.0078$, and $C_e = 0.0028$ when the temperature is 25 °C. Thus, the specific arrangement of the refractive index is $n_{LC} = \text{diag}[n_o, n_o, n_e]$. The basic parameters and values of E_7 are shown in Table 1. The refractive index of LC is higher than that of the background material silica, while the light is introduced into the core of the special fiber, the fiber core is surrounded by air holes with low refractive index, therefore, it can still guide light using total internal reflection. The mode resonance will occur as the phase matching condition is satisfied and the sensing mechanism is based on the coupling between the fiber-core mode and LC mode. The simulation results show that the light-guiding mechanism is not modified by the infiltrated materials.

Table 1. Parameter values of nematic LC E7.

Parameters	Δn (Birefringence)	$\Delta \epsilon$ (Anisotropy)
Values	0.227 (632.8 nm; 20 °C)	12.7 (25 °C; 1 kHz)

Without any electric field, the LC molecules filling the PCF holes are arranged in a planar pattern with their orientation parallel to the fiber axis. As the electric field is exerted, LC molecules will rotate. The angle of rotation can be calculated using Equation (3) [32]:

$$\theta = \begin{cases} 0 & V \leq V_C \\ \frac{\pi}{2} - 2 \tan^{-1} \left[\exp \left(-\frac{V-V_C}{30V_C} \right) \right] & V > V_C \end{cases} \quad (3)$$

where V_C denotes the threshold voltage. Once the threshold voltage is reached, the molecules start to revolve, as Figure 2a depicts. When the voltage is at its saturation value, the rotation angle θ approaches 90°. Figure 2b illustrates the relation between the rotation angle and the ambient voltage.

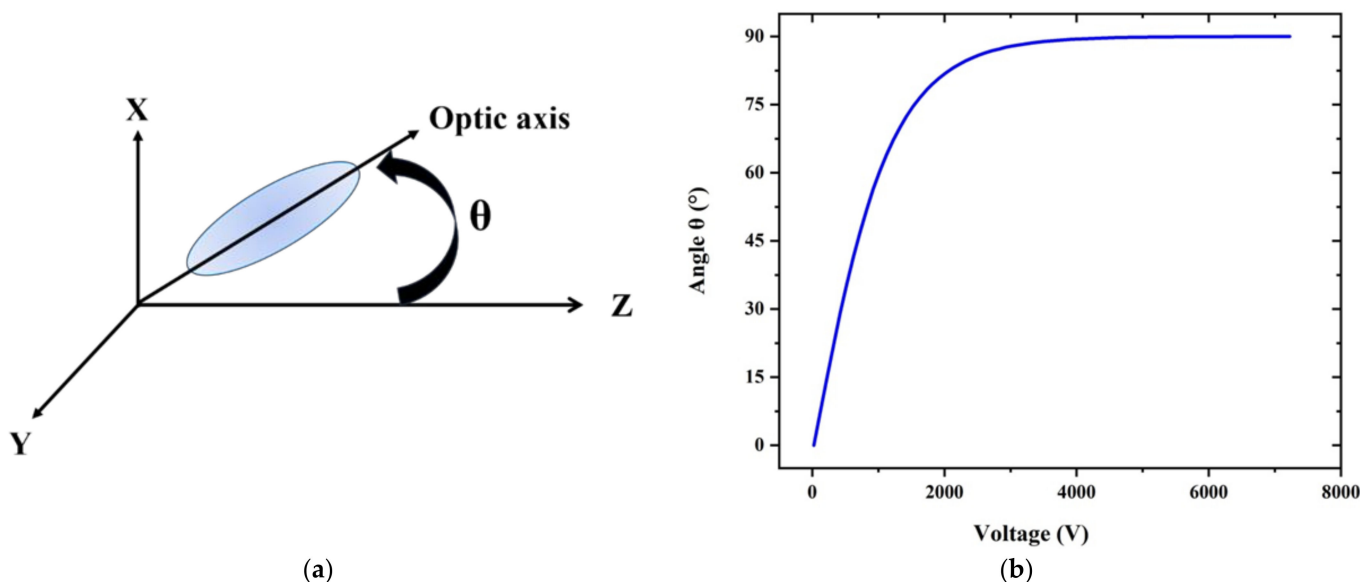


Figure 2. (a) The arrangement of liquid crystal molecules under an external electric field. (b) The relationship between the rotation angle of LC and ambient voltage.

Threshold electric fields could be characterized by [22]:

$$E_C = \frac{\pi}{d} \sqrt{\frac{K11}{\Delta \epsilon}} \quad (4)$$

where $\Delta \epsilon = \epsilon_{\parallel} - \epsilon_{\perp}$, d is the diameter of the filled hole, $K11$ indicates a splay elastic constant of 11.1 pN, the dielectric constant of $\epsilon_{\perp} = 5.2\epsilon_0$ and $\epsilon_{\parallel} = 19.3\epsilon_0$ on the ordinary

y -axis and extraordinary y -axis, respectively, and an electric field with a frequency of 1 kHz is attached. The threshold voltage of LC E₇ is calculated to be 33.83 V. The voltage range from 365 to 565 V is considered in this paper. The permittivity of the diagonal tensor is described by $\varepsilon = \text{diag}[T_{xx}, T_{yy}, T_{zz}]$ [23], where

$$T_{xx} = n_o^2 \quad (5)$$

$$T_{yy} = \cos^2 \theta n_o^2 + \sin^2 \theta n_e^2 \quad (6)$$

$$T_{zz} = \cos^2 \theta n_e^2 + \sin^2 \theta n_o^2 \quad (7)$$

As the voltage becomes higher, the rotation angle θ also becomes larger so we can find that T_{xx} is steady, T_{yy} increases while T_{zz} decreases. It means that the refractive index of the mode in the y direction increases.

3. Results and Discussion

The LC mode and the fiber mode can produce resonance at one wavelength point as the phase fitting condition is satisfied and part of the energy of the fiber mode is captured by the LC mode, therefore, the energy of the fiber mode decreases, reflecting the maximum confinement loss value. As the voltage in the external environment changes, the resonant wavelength would be different. By detecting the offset of the wavelength at the point of maximum losses, the voltage changes can be deduced backwards. The confinement loss of the fiber mode is defined by the equation below [33]:

$$\alpha = 8.686 \times \frac{2\pi}{\lambda} \text{Im}n_{eff} \times 10^6 \quad (8)$$

where λ refers to the operating wavelength in μm , $\text{Im}(n_{eff})$ represents the imaginary portion of effective refractive index, and the losses are calculated using the unit of dB/m.

Figure 3 shows the confinement loss of the fiber mode and the real portion of the effective refractive index of the fiber mode and LC defect mode. We find the refractive indices of both the fiber mode and LC defect mode diminishes as the wavelength grows, while that of the LC defect mode decreases faster, and the two lines intersect at a point. The highest confinement loss is obtained at the resonance wavelength of 1523 nm with an external voltage of 465 V. The fiber mode and LC defect mode couple with each other the strongest when the blue line and the red line are crossed. Here, the peak of the confinement loss of the fiber mode in red spot appears at 880.297 dB/m. This is a spot when the corresponding resonant wavelength is 1523 nm. From then on, they transform into the opponent mode in the x -polarized orientation. The energy of the fiber mode becomes a part of the LC mode instead. The coupling resonance affects the mode field distribution. This is called complete coupling.

Figure 4 shows the confinement loss spectrum of the fiber mode at varying external voltages, ranging from 365 to 565 V, where the temperature is 25 °C. The resonant wavelength for both the fiber mode and LC defect mode shifts along the long wavelength direction, resulting in a red shift. Moreover, it is clearly seen that the intensities of the confinement loss at resonance wavelengths rise with the external electric field increasing. Thus, this mechanism can be effectively utilized for sensing. As the length of the PCF filled with LC is 1 cm, the transmittance is about -10 dB at the resonance wavelength when the confinement loss is 1000 dB/m. If the length of the PCF filled with LC continues to increase, the transmittance will be lower. The length of the PCF filled with LC should be selected according to the practical applications and photoelectric detector.

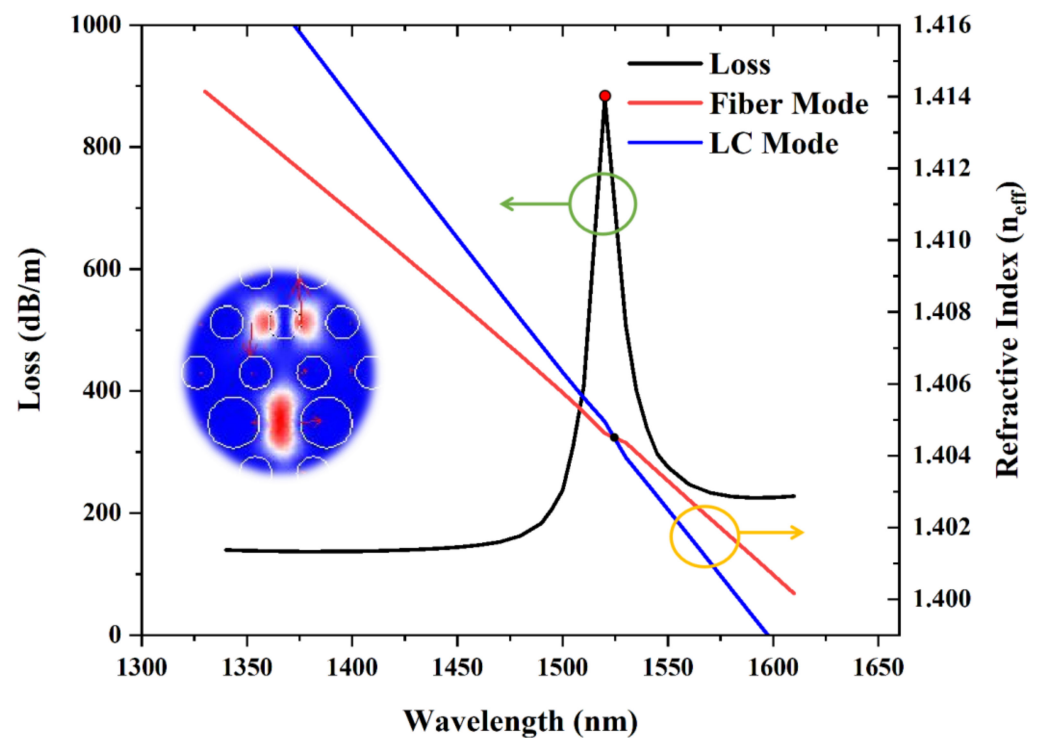


Figure 3. The black curve with green circle for the confinement loss of the fiber mode in the x-polarized direction and the red and blue lines with yellow circle for the variations in the real portion of effective refractive index of the fiber mode and LC defect mode as the external voltage is 465 V. The resonance wavelength is 1523 nm.

The resonant wavelength of the loss spectrum depending on the external voltage is depicted in the Figure 5, the equation of the fitted line is $y = 1.29977x + 914.10649$, and $R^2 = 0.99929$, which means that this PCF voltage sensor possesses a sensitivity of 1.29977 nm/V. Based on the data above, the proposed voltage sensor is highly competent in the voltage measurement field and has a high degree of linearity. Hence, we can easily detect the change in external voltage according to the offset of the resonant wavelength. We chose a higher voltage range from 365 to 565 V. At this range, plenty of industrial settings can be applied such as generation for hydropower stations, power module packages in the automotive industry, and network power supply in railway engineering.

Given the future experiment of this sensing method, the corresponding experimental apparatus were introduced in our previous papers [27,28]. A broadband source and optical spectrum analyzer will be utilized. The ITO glass connected to AC source is utilized to provide a positive polarity voltage waveform with a 1 kHz sinusoidal electrical signal. A polarization controller is utilized to modulate the polarization state of the light. Fiber sensors belong to passive devices. As the functional materials are filled into PCF, strong interaction and mutual coupling occur between light and matter by which the detection precision can be improved.

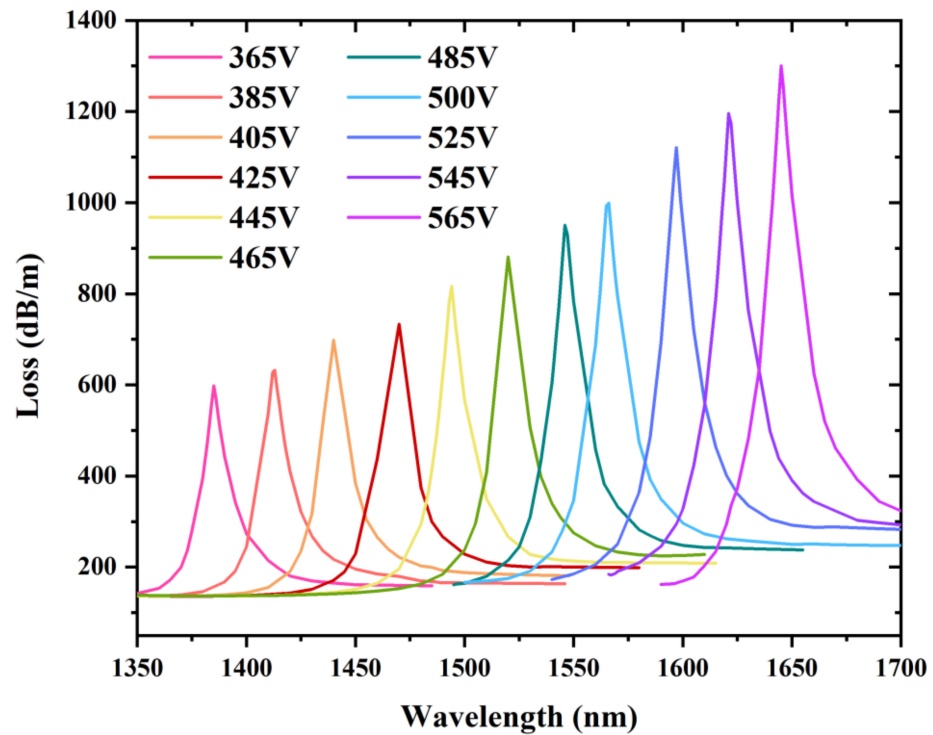


Figure 4. The shift of the loss spectrum of the fiber mode in the x-polarized direction as the voltage increases from 365 to 565 V.

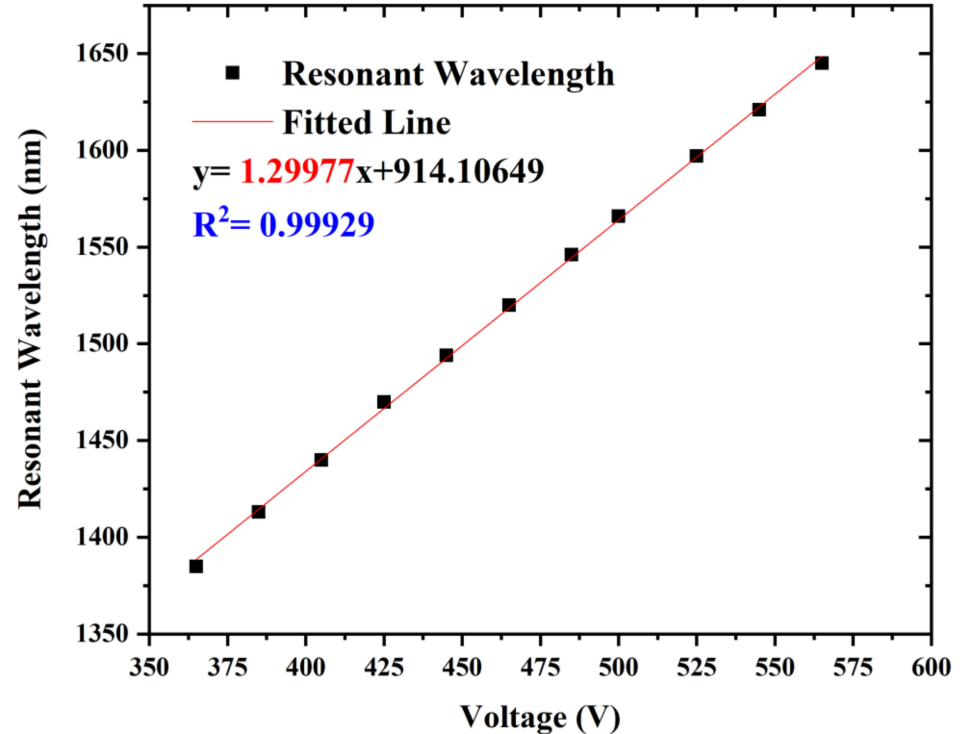


Figure 5. The resonant wavelength of the loss spectrum depending on the external voltage and its fitted line.

4. Temperature Compensation

Considering the Poisson effect of the fiber, optical fiber sensors often have severe temperature cross-sensitivity. Furthermore, the refractive index (RI) of LC is also sensitive to

temperature changing; the corresponding coefficients A , B , and C in Equation (2) at different temperatures are obtained in [31]. Ethanol is a heat-sensitive material and it is particularly sensitive to temperature, whose sensitivity coefficient can reach -4×10^{-4} RIU/°C. The RI of ethanol can be characterized by Equation (9):

$$n = 1.36242 - 4 \times 10^{-4} \times (T - 291.5) \quad (9)$$

where T represents the temperature in Kelvin.

Since the RI of ethanol itself is quite sensitive to temperature changes of the external environment, filling ethanol into the holes of PCF can achieve great sensitivity to temperature measurements. In the structure of the proposed sensor, the LC is influenced by both temperature and voltage, while the ethanol is only influenced by temperature. When LC and ethanol are specifically penetrated into two air holes of PCF, we can detect the corresponding resonant wavelength. The resonant wavelength of the LC-filled fiber shifts beneath diverse electric fields, but the electric fields have no effect on the ethanol-filled one [34]. Nevertheless, the impacts of temperature on the two resonance wavelengths are almost equivalent, leading to the same wavelength shift. Thus, the temperature cross-sensitivity can be removed by computing the discrepancy between the two resonant wavelengths. According to the analysis above, we tried to fill ethanol in the yellow hole in Figure 1, which is in the symmetric position of the LC. Thus, we further present a temperature-compensated voltage sensor based on the differential mode resonance.

The resonant wavelengths shift to the shorter wavelength when the temperature grows, as shown in Figure 6. This is because the refractive indexes of LC mode or ethanol mode decrease with increasing temperature, while the refractive index of the fiber-core mode remains unchanged which leads to the phase matching points shifting to shorter wavelengths. Meanwhile, it can be obviously noticed that the wavelength difference is almost settled, where the surrounding voltage is 465 V. The standard deviation in wavelength difference is less than 2 nm within the temperature adjustment from 25 to 50 °C. The temperature sensitivity is calculated as -3.8 nm/°C. As a result, the proposed sensor can make a great compensation for the temperature variations, thus, conquering the temperature cross-sensitivity of the LC-filled fiber optic voltage sensor.

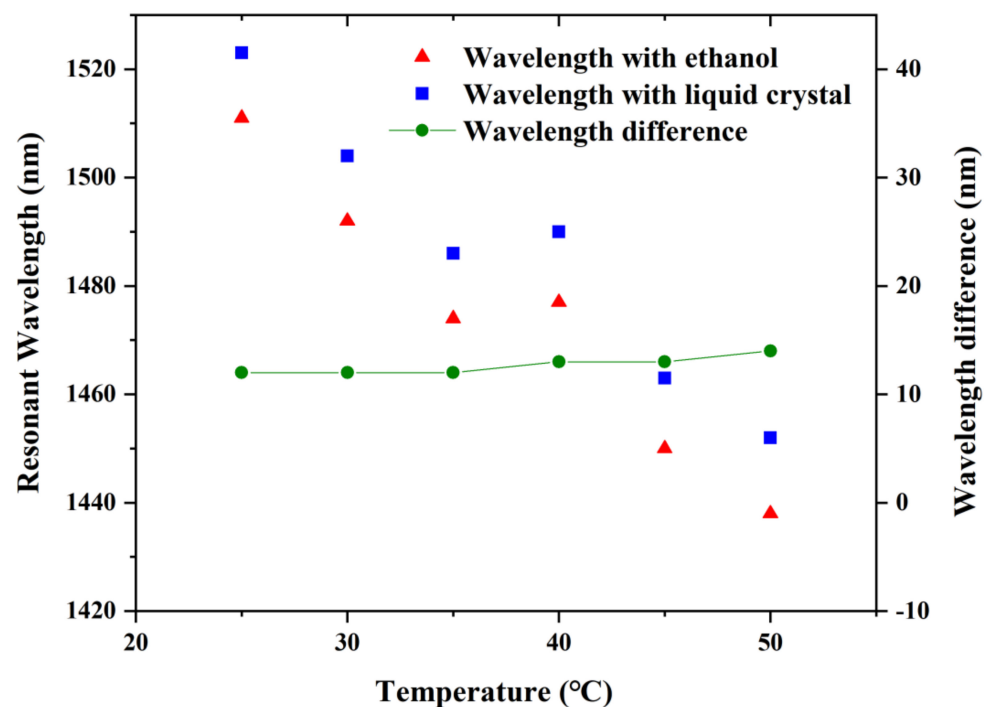


Figure 6. Wavelength shifts of the ethanol- and LC-infiltrated fiber, and wavelength difference between the two resonant wavelengths at the maximum losses.

5. Adjustment of Structural Parameters

Generally, the performances of PCF voltage sensors can be modified by changing their geometrical parameters. The impacts of the geometrical parameters d_1 and d_2 on sensing performance are discussed when the ambient voltages are 465 and 525 V. Moreover, the influences of the spacing of the triangular-lattice distribution Λ on the sensing performances are also discussed for voltages of 465 and 525 V.

5.1. Adjustment of Diameters d_1 and d_2

Figure 7 portrays the variation in the confinement loss with the changes in d_1 while $d = 1.4 \mu\text{m}$, $d_2 = 2.2 \mu\text{m}$, and $\Lambda = 3 \mu\text{m}$ which stay unchanged as ambient voltages are 465 and 525 V. It is clearly observed that the resonance wavelength moves to the longer wavelength when the diameter d_1 is 1.3, 1.4, and 1.5 μm . That is because the RI of the LC defect mode becomes larger while the RI of the fiber mode stays unchanged; thus, achieving a red shift at resonant wavelengths. More energy couples to the LC defect mode for the reason that the LC obtains a greater RI than the background material silica; therefore, confinement losses rise significantly with the increase in the diameter d_1 . In addition, the confinement losses rise on account of the increase in the ambient voltage from 465 to 525 V. At the same time, we can notice that the sensitivity becomes progressively greater with the rising diameter d_1 . We can conclude that the structural parameter d_1 has a significant influence on the sensitivity of this voltage sensor and we could realize better sensing performance by modifying the diameter d_1 of the LC filled hole.

The influence of varying the diameter d_2 of larger air holes in the x-orientation on the resonant wavelength and losses are analyzed. It is obviously illustrated in Figure 8, in which the diameter d_2 is modulated as 2.1, 2.2, and 2.3 μm . Other structural parameters are represented as $d = 1.4 \mu\text{m}$, $d_1 = 1.4 \mu\text{m}$, and $\Lambda = 3 \mu\text{m}$. The resonant wavelength is shifted in the direction of the longer wavelength as the diameter d_2 expands, but this wavelength shift is not as far as that of modifying the diameter d_1 . This is due to the fact that RI of the fiber mode decreases but that of the LC mode remains unchanged, causing the coupling point to red shift. The confinement losses decrease since less energy is transferred into the microstructure cladding due to the increased diameter d_2 of the two larger air holes. The sensitivity increases slightly as we increase the diameter d_2 . Hence, we cannot improve the sensing performance significantly by modulating the diameter d_2 .

5.2. Adjustment of the Spacing Λ

The influence of changing the spacing of the triangular-lattice distribution Λ on the sensing performance is discussed for the voltages of 465 and 525 V. Other construction parameters are maintained as $d = 1.4 \mu\text{m}$, $d_1 = 1.4 \mu\text{m}$, and $d_2 = 2.1 \mu\text{m}$. As shown in Figure 9, it causes a blue shift in the resonant wavelength and confinement loss decreases with the spacing Λ increasing. As a consequence of the index of the fiber mode rising as well as that of the LC defect mode declining, the resonant wavelength shifts in the direction of the shorter wavelength. As spacing Λ becomes larger, less energy couples from the fiber mode to the LC defect mode, resulting in a decrease in losses. It is noticeable that the sensitivity stays essentially unchanged as the spacing Λ changes.

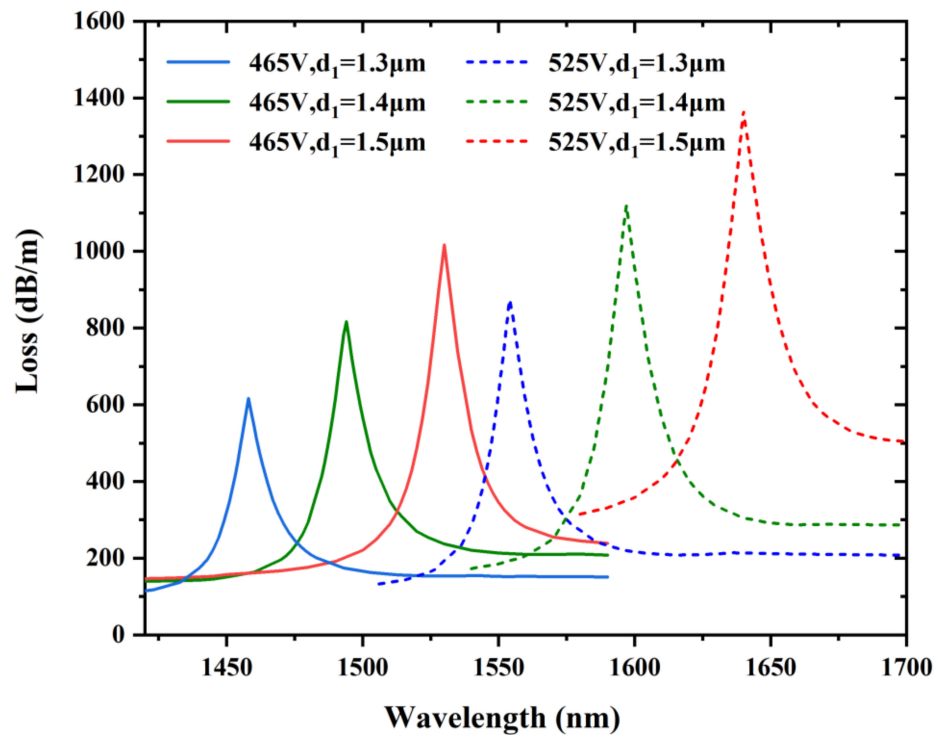


Figure 7. Variation in the confinement loss at the voltages of 465 and 525 V by varying the LC filled hole diameter $d_1 = 1.3, 1.4,$ and $1.5 \mu\text{m}$, while other structural parameters are $d = 1.4 \mu\text{m}$, $d_2 = 2.2 \mu\text{m}$, and $\Lambda = 3 \mu\text{m}$.

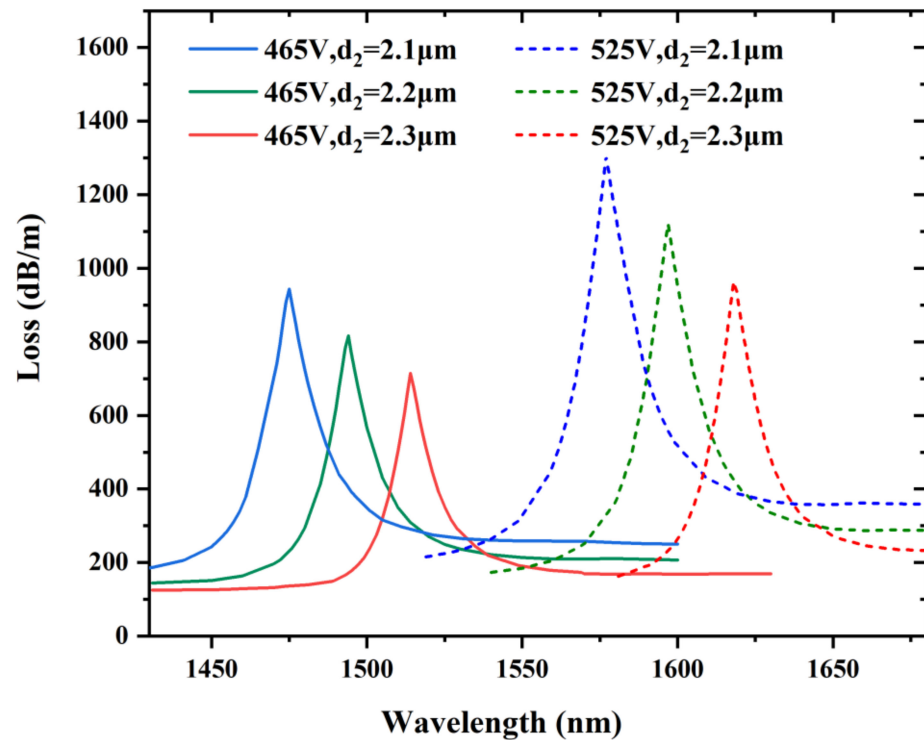


Figure 8. Variation in the confinement loss at the voltages of 465 and 525 V by varying the diameters of the two bigger air holes in the x-direction and $d_2 = 2.1, 2.2,$ and $2.3 \mu\text{m}$, while other structural parameters are $d = 1.4 \mu\text{m}$, $d_1 = 1.4 \mu\text{m}$, and $\Lambda = 3 \mu\text{m}$.

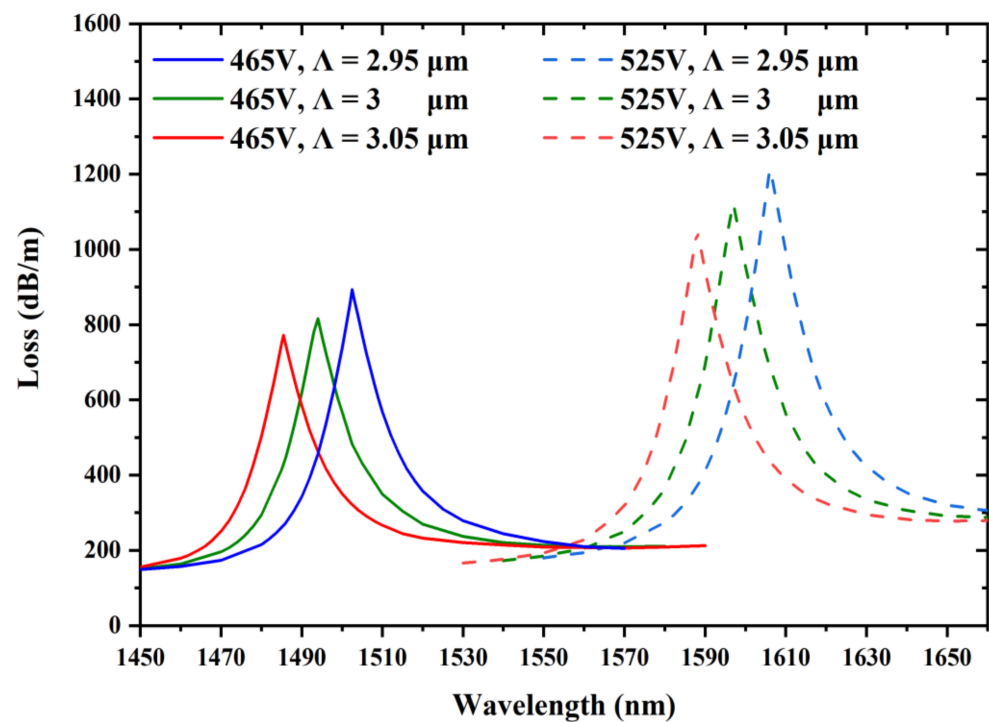


Figure 9. Variation in the confinement loss at the voltages of 465 and 525 V by varying the spacing of the triangular-lattice distribution $\Lambda = 2.95, 3,$ and $3.05 \mu\text{m}$, while other structural parameters are $d = 1.4 \mu\text{m}$, $d_1 = 1.4 \mu\text{m}$, and $d_2 = 2.1 \mu\text{m}$.

6. Conclusions

In this paper, a mode-coupling voltage sensor based on LC-filled photonic crystal fiber was presented and analyzed based on the finite element method. The characteristics of LC vary with different ambient voltages. By calculating and analyzing the confinement loss and the shift of the resonant wavelength as the voltage ranges from 365 to 565 V, the sensor reached a sensitivity of 1.29977 nm/V at the temperature of $25 \text{ }^\circ\text{C}$. One hole of the PCF was infiltrated with ethanol which was merely sensitive to temperature to realize the temperature compensation. The standard deviation of the wavelength difference was less than 2 nm within the temperature adjustment from 25 to $50 \text{ }^\circ\text{C}$. Moreover, we tried to adjust the relevant structural parameters for better sensing performance. In conclusion, the proposed temperature-compensated voltage sensor is promising in the voltage sensing field and possesses good prospects for applications.

Author Contributions: W.-L.W.: Conceptualization, investigation, writing—original draft. Q.L.: Writing—review and editing, funding acquisition, resources, project administration. Z.-Y.L.: Methodology. Q.W.: Supervision. Y.-Q.F.: Supervision. All authors have read and agreed to the published version of the manuscript.

Funding: This research was funded by the National Natural Science Foundation of China (Grant No. 51907017), the Key Science and Technology Research Projects of Higher Education Institutions in Hebei Province of China (Grant No. ZD2019304), Hebei Natural Science Foundation (Grant No. F2020501040), and the Fundamental Research Funds for the Central Universities of China (Grant No. N2123012).

Institutional Review Board Statement: Not applicable.

Informed Consent Statement: Not applicable.

Data Availability Statement: Not applicable.

Conflicts of Interest: The authors declare no conflict of interest.

References

1. Birks, T.A.; Roberts, P.J.; Russell, P.S.J.; Atkin, D.M.; Shepherd, T.J. Full 2-D photonic bandgaps in silica/air structures. *Electron. Lett.* **1995**, *31*, 1941–1943. [[CrossRef](#)]
2. Yu, X.; Sun, Y.; Ren, G.B.; Shum, P.; Ngo, N.Q.; Kwok, Y.C. Evanescent field absorption sensor using a pure-silica defected-core photonic crystal fiber. *IEEE Photon. Technol. Lett.* **2008**, *20*, 336–338. [[CrossRef](#)]
3. Pierce, J.R. Coupling of modes of propagation. *J. Appl. Phys.* **1954**, *25*, 179–183. [[CrossRef](#)]
4. Snyder, A.W. Coupled-mode theory for optical fibers. *J. Opt. Soc. Am.* **1972**, *62*, 1267–1277. [[CrossRef](#)]
5. Marcuse, D. Coupled mode theory of round optical fibers. *Bell Syst. Tech. J.* **1973**, *52*, 817–842. [[CrossRef](#)]
6. Yariv, A. Coupled-mode theory for guided-wave optics. *IEEE J. Quantum Electron.* **1973**, *9*, 919–933. [[CrossRef](#)]
7. Taylor, H.F. Optical switching and modulation in parallel dielectric waveguides. *J. Appl. Phys.* **1973**, *44*, 3257–3262. [[CrossRef](#)]
8. Kogelnik, H.; Schmidt, R.V. Switched directional couplers with alternating ΔB . *IEEE J. Quantum Electron.* **1976**, *12*, 396–402. [[CrossRef](#)]
9. Noda, J.; Fukuma, M.; Mikami, O. Design calculations for directional couplers fabricated by Ti-diffused LiNbO₃ waveguides. *Appl. Opt.* **1981**, *20*, 2284–2290. [[CrossRef](#)]
10. McIntyre, P.D.; Snyder, A.W. Power transfer between optical fibers. *J. Opt. Soc. Am.* **1973**, *63*, 1518–1527. [[CrossRef](#)]
11. Kogelnik, H.; Shank, C.V. Coupled-wave theory of distributed feedback lasers. *J. Opt. Soc. Am. B.* **1972**, *43*, 2327–2335. [[CrossRef](#)]
12. Heavens, O.S. Principles of Optics. By Born and Wolf. 1964. (Pergamon). *Math. Gaz.* **1965**, *49*, 485. [[CrossRef](#)]
13. Larsen, T.T.; Bjarklev, A.; Hermann, D.S.; Broeng, J. Optical devices based on liquid crystal photonic bandgap fibres. *Opt. Express* **2003**, *11*, 2589–2596. [[CrossRef](#)] [[PubMed](#)]
14. Wei, L.; Alkeskjold, T.T.; Bjarklev, A. Compact design of an electrically tunable and rotatable polarizer based on a liquid crystal photonic bandgap fiber. *IEEE Photon. Technol. Lett.* **2009**, *21*, 1633–1635. [[CrossRef](#)]
15. Hu, J.; Fu, D.; Xia, C.; Long, S. Fiber Mach-Zehnder-interferometer-based liquid crystal biosensor for detecting enzymatic reactions of penicillinase. *Appl. Opt.* **2019**, *58*, 4806–4811. [[CrossRef](#)]
16. Chu, W.S.; Kim, S.M.; Wu, X.; Wen, L.; Oh, M.C. Optical voltage sensors based on integrated optical polarization-rotated reflection interferometry. *J. Lightwave Technol.* **2016**, *34*, 2170–2174. [[CrossRef](#)]
17. Pan, F.; Xiao, X.; Xu, Y.; Ren, S. An optical AC voltage sensor based on the transverse pockels effect. *Sensors* **2011**, *11*, 6593–6602. [[CrossRef](#)]
18. Zhu, T.; Ou, Z.; Han, M.; Deng, M.; Chiang, K.S. Propylene carbonate based compact fiber Mach-Zehnder interferometric electric field sensor. *J. Lightwave Technol.* **2013**, *31*, 1566–1572. [[CrossRef](#)]
19. Chen, X.; He, S.; Li, D.; Wang, K.; Fan, Y.; Wu, S. Optical fiber voltage sensor based on Michelson Interferometer using phase generated carrier demodulation algorithm. *IEEE Sens. J.* **2015**, *16*, 349–354. [[CrossRef](#)]
20. Marignetti, F.; Santis, E.; Avino, S.; Tomassi, G.; Giorgini, A.; Malara, P.; De Natale, P.; Gagliardi, G. Fiber bragg grating sensor for electric field measurement in the end windings of high-voltage electric machines. *IEEE Trans. Ind. Electron.* **2016**, *36*, 2796–2802. [[CrossRef](#)]
21. Wang, P.; Semenova, Y.; Wu, Q.; Farrell, G.A. Fiber-Optic voltage sensor based on macrobending structure. *Opt. Laser Technol.* **2011**, *43*, 922–924. [[CrossRef](#)]
22. Haakestad, M.W.; Alkeskjold, T.T.; Nielsen, M.D.; Scolari, L.; Riishede, J.; Engan, H.E.; Bjarklev, A. Electrically tunable photonic bandgap guidance in a liquid-crystal-filled photonic crystal fiber. *IEEE Photon. Technol. Lett.* **2005**, *17*, 819–821. [[CrossRef](#)]
23. Ertman, S.; Wolinski, T.R.; Pysz, D.; Buczynski, R.; Nowinowski-Kruszelnicki, E.; Dabrowski, R. Low-loss propagation and continuously tunable birefringence in high-index photonic crystal fibers filled with nematic liquid crystals. *Opt. Express.* **2009**, *17*, 19298–19310. [[CrossRef](#)] [[PubMed](#)]
24. Du, J.; Liu, Y.; Wang, Z.; Zou, B.; Liu, B.; Dong, X. Electrically tunable Sagnac filter based on a photonic bandgap fiber with liquid crystal infused. *Opt. Lett.* **2008**, *33*, 2215. [[CrossRef](#)]
25. Huang, Y.; Wang, Y.; Zhang, L.; Shao, Y.; Zhang, F.; Liao, C.; Wang, Y. Tunable electro-optical modulator based on a photonic crystal fiber selectively filled with liquid crystal. *J. Lightwave Technol.* **2019**, *37*, 1903–1908. [[CrossRef](#)]
26. Liu, Q.; Xue, P.; Liu, Z. Voltage sensor based on liquid-crystal-infiltrated photonic crystal fiber with high index. *Appl. Phys. Express.* **2020**, *13*, 032005. [[CrossRef](#)]
27. Liu, Q.; Xue, P.; Wu, Q.; Zhao, C.; Ng, W.P.; Fu, Y.; Binns, R. Electrically sensing characteristics of the sagnac interferometer embedded with a liquid crystal-infiltrated photonic crystal fiber. *IEEE Trans. Instrum. Meas.* **2021**, *70*, 1–9. [[CrossRef](#)]
28. Xue, P.; Liu, Q.; Wu, Z.; Wu, Q.; Zhao, C.; Ng, W.P.; Fu, R.; Binns, R. Electrically tuning characteristics of LC selectively infiltrated PCF Sagnac interferometer. *IEEE Photon. Technol. Lett.* **2021**, *33*, 668–671. [[CrossRef](#)]
29. Wang, Y.; Liao, C.R.; Wang, D.N. Femtosecond laser-assisted selective infiltration of microstructured optical fibers. *Opt. Express.* **2010**, *18*, 18056–18060. [[CrossRef](#)]
30. Malitson, I.H. Inter specimen comparison of the refractive index of fused silica. *J. Opt. Soc. Am.* **1965**, *55*, 1205–1209. [[CrossRef](#)]
31. Li, J.; Wu, S.T.; Brugioni, S.; Meucci, R.; Faetti, S. Infrared refractive indices of liquid crystals. *J. Appl. Phys.* **2005**, *97*, 073501. [[CrossRef](#)]
32. Wang, E.; Jiang, H.; Xie, K.; Chen, C.; Hu, Z. Polarization splitter based on dual core liquid crystal-filled holey fiber. *J. Appl. Phys.* **2016**, *120*, 114501. [[CrossRef](#)]

33. Hassani, A.; Skorobogatiy, M. Design criteria for microstructured-optical-fiber-based surface-plasmon-resonance sensors. *J. Opt. Soc. Am.* **2007**, *24*, 1423–1429. [[CrossRef](#)]
34. Gao, R.; Lu, D.; Cheng, J.; Jiang, Y.; Qi, Z. Temperature-compensated fibre optic magnetic field sensor based on a self-referenced anti-resonant reflecting optical waveguide. *Appl. Phys. Lett.* **2017**, *110*, 131903. [[CrossRef](#)]